

Spatial distribution of radionuclides in 3D models of SN 1987A and Cas A

Hans-Thomas Janka¹, Michael Gabler² and Annop
Wongwathanarat^{1,3}

¹Max Planck Institute for Astrophysics,
Postfach 1317, D-85741 Garching, Germany
email: thj@mpa-garching.mpg.de

²Max Planck Institute for Astrophysics,
Postfach 1317, D-85741 Garching, Germany
email: miga@mpa-garching.mpg.de

³RIKEN, Astrophysical Big Bang Laboratory,
2-1 Hirosawa, Wako, Saitama 351-0198, Japan
email: annop.wongwathanarat@riken.jp

Abstract. Fostered by the possibilities of multi-dimensional computational modeling, in particular the advent of three-dimensional (3D) simulations, our understanding of the neutrino-driven explosion mechanism of core-collapse supernovae (SNe) has experienced remarkable progress over the past decade. First self-consistent, first-principle models have shown successful explosions in 3D, and even failed cases may be cured by moderate changes of the microphysics inside the neutron star (NS), better grid resolution, or more detailed progenitor conditions at the onset of core collapse, in particular large-scale perturbations in the convective Si and O burning shells. 3D simulations have also achieved to follow neutrino-driven explosions continuously from the initiation of the blast wave, through the shock breakout from the progenitor surface, into the radioactively powered evolution of the SN, and towards the free expansion phase of the emerging remnant. Here we present results from such simulations, which form the basis for direct comparisons with observations of SNe and SN remnants in order to derive constraints on the still disputed explosion mechanism. It is shown that predictions based on hydrodynamic instabilities and mixing processes associated with neutrino-driven explosions yield good agreement with measured NS kicks, light-curve properties of SN 1987A and asymmetries of iron and ⁴⁴Ti distributions observed in SN 1987A and Cassiopeia A.

Keywords. supernovae: general, supernovae: individual (Cassiopeia A, SN1987A), neutrinos, hydrodynamics, instabilities, nuclear reactions, nucleosynthesis, abundances

1. Introduction

Since the seminal works by Colgate & White (1966) and Arnett (1967) more than 50 years ago, the computational modeling of supernova (SN) explosions has experienced enormous progress with respect to the numerical methods, input physics, computational accuracy, and dimensionality. Nevertheless, despite many generations of successively improved simulations, initially performed in spherical symmetry (1D), then since the 1990's also in two dimensions (2D), and in recent years also in full 3D, the physical processes that cause the explosion are not established yet (for recent reviews, see Janka (2012), Burrows (2013), Foglizzo et al. (2015), Janka et al. (2016), Müller (2016), Janka (2017b)). For the far majority of normal core-collapse SNe the delayed neutrino-driven mechanism (Wilson (1985), Bethe & Wilson (1985)) is widely considered as most likely explanation, because it taps the vast reservoir of energy that is radiated by the nascent neutron star (NS) in neutrinos and outranges the explosion energy of SNe by a factor of several hundred.

The neutrino-driven mechanism also satisfies a number of fundamental requirements that any viable scenario should fulfill (for a detailed discussion, see Janka (2017b)). First, the mechanism is *not* “robust”, because it should allow for the formation of stellar-mass black holes (BHs), whose abundant existence has been confirmed by the recent measurements of gravitational waves from binary BH mergers (Abbott et al. (2016)). Second, it must be *inefficient*, because it should explain why SN explosion energies are so much lower than the gigantic amount of gravitational binding energy that is available during NS or BH formation. Third, it should be *self-regulated*, because the energy transferred to the ejecta does not largely exceed the binding energy of the progenitor shells outside of the degenerate core, i.e., it is as low as several 10^{49} erg to about 10^{50} erg near the low-mass side of SN progenitors and may be $\sim(1 - 2) \times 10^{51}$ erg for energetic explosions of stars around $20 M_{\odot}$. This clearly separates such normal SNe from the significantly more powerful but much rarer hypernovae (with a rate of less than roughly one out of thousand core-collapse events), whose energies and explosion properties point to another mechanism, probably invoking the formation of BHs or magnetars and of jet-driven outflows caused by extreme amplification of magnetic fields during the collapse of rapidly rotating progenitors (see, e.g., Woosley & Bloom (2006)). The latter are the final outcome of very special and uncommon single and binary star evolution scenarios of massive stars (e.g., Levan et al. (2016)).

Although first 3D simulations with energy-dependent neutrino transport have meanwhile obtained successful explosions by neutrino heating (Takiwaki et al. (2014), Melson et al. (2015a), Melson et al. (2015b), Lentz et al. (2015), Roberts et al. (2016), Müller (2016)), the viability of this theoretical scenario is still not generally accepted (e.g., Soker (2017a), Soker (2017b), Kushnir & Katz (2015), Blum & Kushnir (2016)). Doubts are either motivated by referring to those computational models where the numerical setups still failed to produce explosions, or they are justified by pointing to remaining shortcomings of the current calculations, for example the lack of a clear demonstration by modern simulations that neutrino-driven explosions can yield energies around 10^{51} erg or more (e.g., Soker (2017a) and references therein). Such missing pieces in the puzzle are very likely to fall into place once longer and better resolved 3D simulations are performed, larger sets of progenitors are investigated, more consistent initial conditions that account for large-scale perturbations in the convective silicon and oxygen burning shells are applied (Couch & Ott (2013), Couch et al. (2015), Müller & Janka (2015), Müller (2016)), and further improvements of the microphysics are used for the description of dense NS matter and of neutrino interactions in the correlated nuclear medium (see the sensitivity test by Melson et al. (2015b)).

Moreover, convincing alternatives to the neutrino-heating mechanism, which could elucidate the processes that initiate and power most core-collapse SNe, do not exist. Considering thermonuclear burning in the stellar carbon shell during gravitational collapse as the main energy source of the SN blast wave (Kushnir & Katz (2015)) demands a radical change of the chemical structure of progenitor stars in conflict with the results of stellar evolution calculations. This approach to overrule the common notion of stellar evolution appears as an unnecessary and overmotivated act of desperation. Similarly unsatisfactory (and not particularly elegant) is a renunciation of self-consistency in the explosion modeling by introducing, in an ad hoc manner, components whose physical origin remains unexplained, for example “jittering jets” (Soker (2017a) and references therein). Magnetic fields, which are often readily invoked to bridge gaps of reasoning, cannot be made responsible for the production of (jittering) jets in most or even in all SNe as claimed by Soker (2017a). Many stellar collapse simulations including the effects of magnetic fields (e.g., Moiseenko & Bisnovatyi-Kogan (2007), Burrows et al. (2007), Mösta et al.

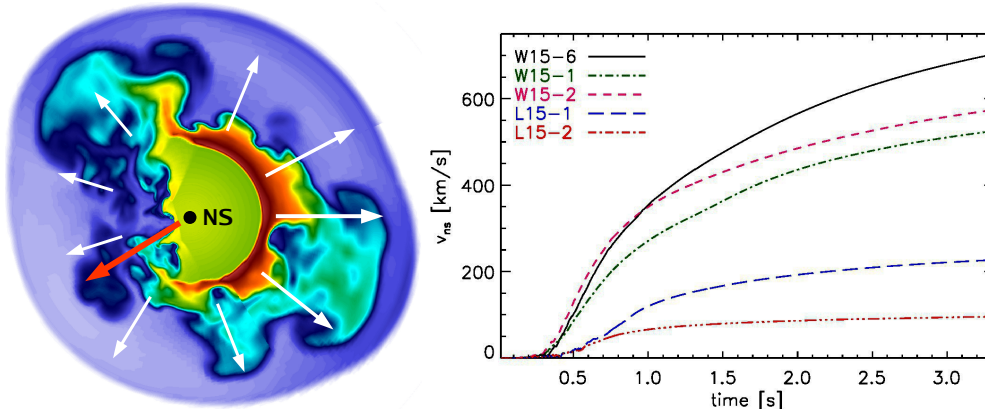


Figure 1. *Left:* Mass ejection asymmetry in a cross-sectional plane for one of the 3D simulations of neutrino-driven explosions (at 1.3s after core bounce) published by Wongwathanarat et al. (2013). The NS kick direction (marked by the red arrow) is opposite to the hemisphere of the stronger explosion, where relatively more mass from silicon to the iron group is expelled. The entropy per nucleon is color coded (blue, green, yellow, red signal growing values), and the outer contour is the deformed SN shock. *Right:* NS star kick velocities as functions of time for a subset of the 3D simulations of neutrino-driven explosions in Wongwathanarat et al. (2013).

(2014), Mösta et al. (2015), Obergaulinger & Aloy (2017)) have demonstrated that very rapid rotation of the progenitor cores is needed to obtain magnetohydrodynamic jets by field amplification. The thus required angular momentum in stellar cores is in conflict with the moderate spin rates of white dwarfs (Kawaler (2015)) and young neutron stars (Heger et al. (2000), Heger et al. (2005)), with predictions from stellar evolution calculations including angular momentum transport through magnetic fields for progenitors of normal core-collapse SNe (Heger et al. (2005)), and with astroseismological measurements, which find core rotation rates that are considerably *slower* than predicted by the stellar evolution models (e.g., Beck et al. (2012), Eggenberger et al. (2012), Eggenberger et al. (2016)). Angular momentum separation in collapsed stellar cores by spiral modes of the standing accretion shock instability (SASI), which can develop even in nonrotating stars (e.g. Kazeroni et al. (2017)), has been shown to potentially lead to considerable growth of the initial B-fields (Endeve et al. (2012)). However, the emerging field configuration is highly turbulent and does not possess the ordered structure on large scales that is necessary for driving jet outflows. This problem will not disappear by future 3D simulations with increased grid refinement, because better resolution of the turbulent flow will foster a growth of the fields on *small scales* while it is unlikely to boost a large-scale field that could enable jet formation.

Despite these direct and indirect arguments in favor of neutrino-driven explosions, this theoretical scenario requires further consolidation by demonstrating that corresponding explosion models are able to account for the observational properties of SNe and of their remnants. In the following, a number of such aspects will be briefly summarized that provide support for the neutrino-driven mechanism.

2. Neutrino-driven explosions: 3D models versus observations

In the following we present some selected results from recent 3D calculations of neutrino-driven explosions that were performed with the PROMETHEUS-HOTB code for different red (RSG) and blue supergiants (BSG) of $15 M_{\odot}$ and $20 M_{\odot}$ by Wongwathanarat et al.

(2013), Wongwathanarat et al. (2015), Wongwathanarat et al. (2016). The blast waves were artificially initiated with a parametric neutrino “engine” such that explosion energies in the ballpark of quite energetic SNe like SN 1987A and Cassiopeia A were obtained. Although the modeling is not based on a fully self-consistent first-principle approach, the simulations still capture the essential physics of neutrino-driven explosions, which start by the energy deposition of neutrinos around the newly formed NS and succeed by the crucial support of hydrodynamic instabilities (convective overturn and SASI), creating large-scale asymmetries in the outgoing SN shock and the innermost ejecta already during the very first second of the explosion. The subsequent SN evolution is then followed continuously from core bounce to shock breakout at the progenitor surface and beyond (see the contribution in this volume by M. Gabler et al.).

Neutron-star kicks. The asymmetric onset of the explosion causes momentum transfer to the newly formed NS mainly by the long-time gravitational interaction between the compact remnant and the anisotropically expelled matter (Scheck et al. (2006), Wongwathanarat et al. (2013)). This leads to NS kicks opposite to the direction of the stronger explosion (consistent with linear momentum conservation in the disrupted star; Fig. 1, left). The kick velocities v_{ns} cover the full range of measured space velocities of young NSs up to nearly 1000 km s^{-1} (Fig. 1, right):

$$v_{\text{ns}} = 211 \frac{\text{km}}{\text{s}} \zeta \left(\frac{\alpha_{\text{ej}}}{0.1} \right) \left(\frac{E_{\text{exp}}}{10^{51} \text{ erg}} \right) \left(\frac{M}{1.5 M_{\odot}} \right)^{-1}, \quad (2.1)$$

(Janka (2017a)), where α_{ej} is the momentum-asymmetry of the innermost ejecta, E_{exp} the explosion energy, M the NS mass, and ζ is a numerical factor of order unity. α_{ej} is determined by stochastic effects during the onset of the asymmetric explosion. While it is found to vary usually between 0 and ~ 0.3 in existing 2D and 3D SN models, higher values are well possible, and kick velocities in excess of 1000 km s^{-1} seem in reach for extreme explosions with high energies and large asphericities.

Light curve of SN 1987A. The initial ejecta asymmetries, which are caused by the neutrino-driven mechanism and its associated hydrodynamic instabilities, lead to a global asphericity of the explosion. They also trigger efficient growth of secondary Rayleigh-Taylor (RT) instabilities at the C-O/He and He/H shell interfaces of the progenitor by crossing density and pressure gradients after the passage of the outgoing shock (for a detailed discussion, see Wongwathanarat et al. (2015)).

These RT instabilities induce the fragmentation of the initial large-scale structures and

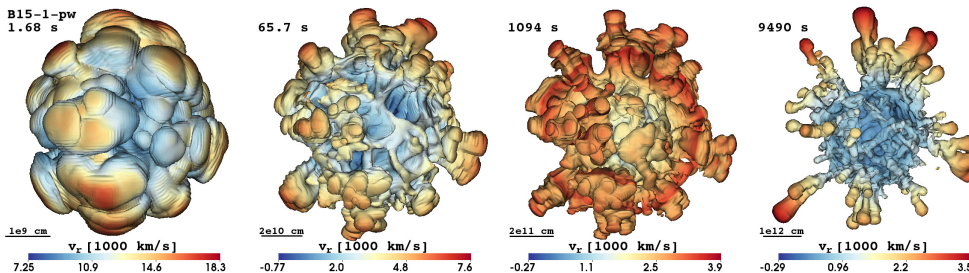


Figure 2. Fragmentation and growth of initial explosion asymmetries by secondary Rayleigh–Taylor instabilities at the C-O/He and He/H composition interfaces for a $15 M_{\odot}$ BSG star. The images show isosurfaces for a mass-fraction of 3% iron-group elements at the time when the SN shock crosses the C-O/He and He/H interfaces (*left* and *second*, respectively), before the reverse shock from the He/H interface hits the iron ejecta (*third*), and at shock breakout (*right*). (Images from Wongwathanarat et al. (2015))

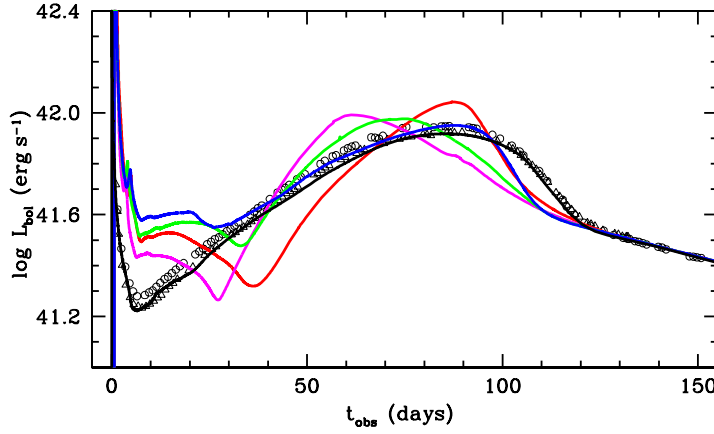


Figure 3. Bolometric light curves for SN calculations of four BSG progenitors (solid colored lines) compared to the observed light curve of SN 1987A (symbols; see Utrobin et al. (2015)). The neutrino-driven explosions from shock-formation until beyond shock breakout were simulated in 3D, while the long-time radiation-hydrodynamical light-curve calculations were carried out in 1D, starting from spherically averaged data of the 3D explosion models. The blue line corresponds to the model shown in Fig. 2, where strong outward mixing of radioactive nickel and inward mixing of hydrogen allow for a good reproduction of the light-curve peak of SN 1987A. The imperfect match around the luminosity minimum and during the decline phase from the peak is a consequence of an overestimated radius and underestimated ejecta mass by the progenitor model. The black line corresponds to a specifically tailored stellar model.

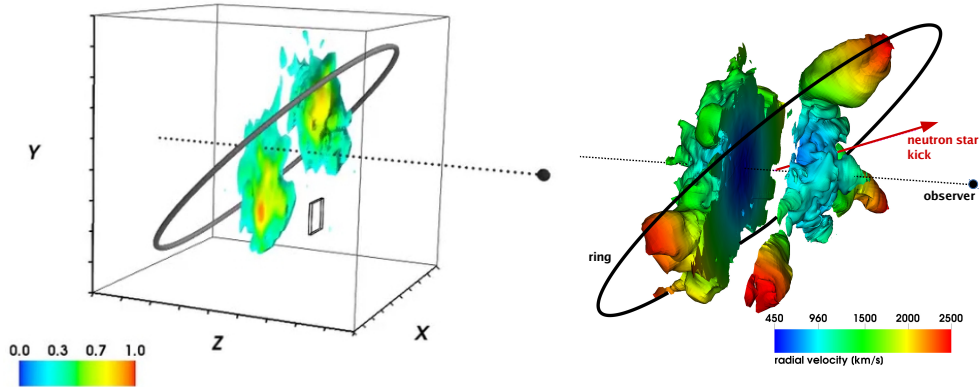


Figure 4. *Left:* 3D isosurfaces for $[\text{SiII}] + [\text{FeII}]$ in SN 1987A, combining the levels for 30%, 50%, and 70% of the maximal intensity as indicated by the color bar from Larsson et al. (2016). The ring corresponds to the position of the reverse shock at the inner edge of the equatorial ring, and the dotted line marks the viewing direction with the observer location indicated by the filled circle. Tick marks on the axes are spaced in intervals of 1000 km s^{-1} . *Right:* Similar visualization of the iron distribution in a 3D neutrino-driven explosion simulation with an energy close to that of SN 1987A. The explosion has been evolved to 600 days including heating by ^{56}Ni decay. The image shows an isosurface of constant mass-density of ^{56}Fe with the radial velocity color coded. Including silicon yields a very similar morphology but higher velocities. As in the observation, the central region within $\pm 450 \text{ km s}^{-1}$ along the line of sight has been removed. The observer direction (dashed line with bullet for observer position) was chosen for optimal similarity with the observations; the corresponding ring plane and the NS kick direction of the SN model are also indicated.

counteract the deceleration of the inner ejecta by the reverse shock that moves into the metal core. As a consequence, effective outward mixing of radioactive ^{56}Ni (in extended finger-like plumes with velocities up to $\sim 3500 \text{ km s}^{-1}$, see Fig. 2) and inward mixing of hydrogen (to velocities close to zero) can take place. 3D simulations of neutrino-driven explosions are thus able to account for the radial mixing and high nickel velocities that are needed to explain the shape of the light curve of SN 1987A (Fig. 3), the early observations of gamma-rays and X-rays from radioactive decays, and a variety of spectral features of this SN (Arnett et al. (1989) and references therein).

Silicon and iron ejecta in SN 1987A. Based on detailed spectral and imaging observations with HST/STIS and VLT/SINFONI, Larsson et al. (2016) produced 3D maps of various chemical components of SN 1987A including silicon and iron. The morphology of these tracers of the innermost ejecta is shown in the left panel of Fig. 4. In the right panel of this figure we display the iron distribution (Si+Fe only differs insignificantly) in a 3D neutrino-driven explosion model for a $15 M_{\odot}$ star with properties (energy, ejecta geometry) resembling those of SN 1987A. We only display the dense, inner regions of the iron material up to radial velocities of 2500 km s^{-1} , guided by the space velocities of the centers of the brightest regions in the left panel. Moreover, following the observational image we also omit all mass with velocities between -450 km s^{-1} and $+450 \text{ km s}^{-1}$ along the line of sight. Assuming that 15–30% of high-velocity Fe and Si, of which some are in extended fingers similar to those in Fig. 4, remain invisible is justified for three reasons: First, although such high-velocity material is not seen in the observations, it *must* be present in SN 1987A to explain its light curve and spectral properties (see above). Second, the fingers and plumes of high-velocity Si and Fe possess an average mass-density that is at least a factor of 10 lower than the density of the central bulk of iron. Third, the observed $[\text{SiI}]+[\text{FeII}]$ emission is powered by positrons from ^{44}Ti decay (Larsson et al. (2016)), but titanium in the extended plumes is less abundant (at least a factor of 2) relative to iron than in the more concentrated, lower-velocity bulk. Therefore, the excitation of Si and Fe by ^{44}Ti -decay positrons must be expected to be less efficient. The resemblance of the two images in Fig. 4 is assuring, in particular since the 3D simulation was *not tailored* to match SN 1987A.

^{44}Ti and iron in Cassiopeia A. Using NuSTAR observations Grefenstette et al. (2014) and Grefenstette et al. (2017) mapped the 3D distribution of ^{44}Ti in Cas A, which is a perfect tracer of the explosion geometry of this SN. They found a clumpy, non-uniform distribution of titanium around the centre of expansion with most of the high-emission ^{44}Ti knots being concentrated in the hemisphere opposite to the NS kick direction. Without any fine tuning, one of the 3D neutrino-driven explosion simulations of Wongwathanarat et al. (2015) is able to account for the main properties of the observed titanium and iron distributions (Figs. 5 and 6; Wongwathanarat et al. (2016)). The theoretical model can explain the total yields of these nuclei estimated for Cas A, their 3D geometry in relation to the NS kick magnitude and direction, their radial and velocity distributions, and the relative variations of the ^{44}Ti /iron ratio suggested by the observations. The morphology of this explosion seems to be compatible with a neutrino-driven explosion that produced three large-scale plumes of neutrino-heated, high-entropy ejecta that are essentially located in one plane (Wongwathanarat et al. (2016)), which could be associated with the “tilted thick disk” identified in Cas A (see Grefenstette et al. (2017)).

3. Conclusions

Neutrino-driven explosion simulations in 3D can explain basic observational properties of the distribution of the innermost ejecta (iron-group material, radioactive ^{44}Ti) ob-

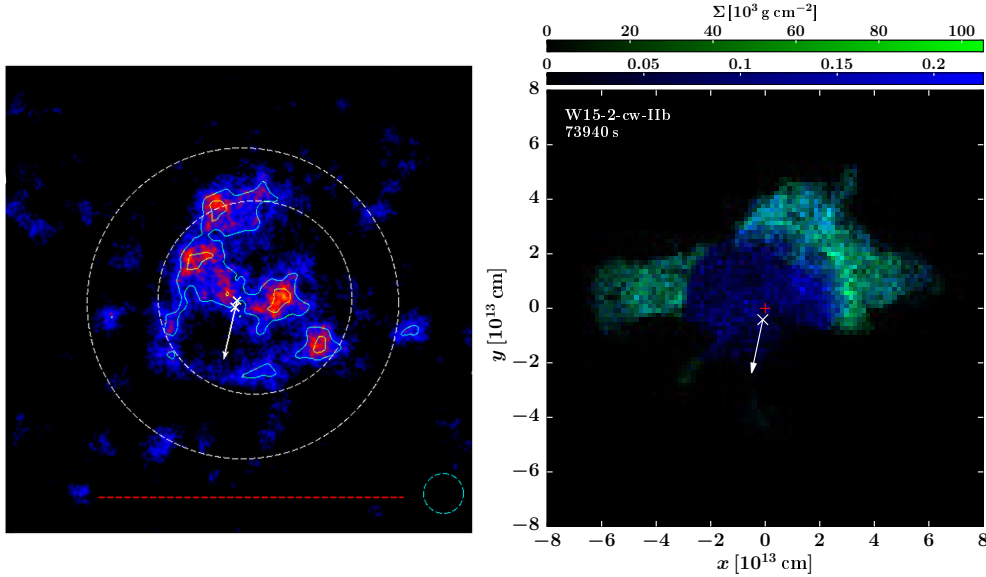


Figure 5. *Left:* ^{44}Ti distribution in Cas A with forward and reverse shock locations marked by dashed circles (reprinted by permission from Macmillan Publishers Ltd: Nature, Grefenstette et al. (2014), ©2014). *Right:* Distribution of ^{44}Ti (blue) and ^{56}Fe (decay product of ^{56}Ni) in a 3D simulation of a neutrino-driven explosion (Wongwathanarat et al. (2016)). The reverse shock is assumed to have moved inward through half of the iron, which is therefore visible and displayed only in the shock-heated outer shell. In both images the geometrical center of the expansion and the location and kick direction of the NS are indicated.

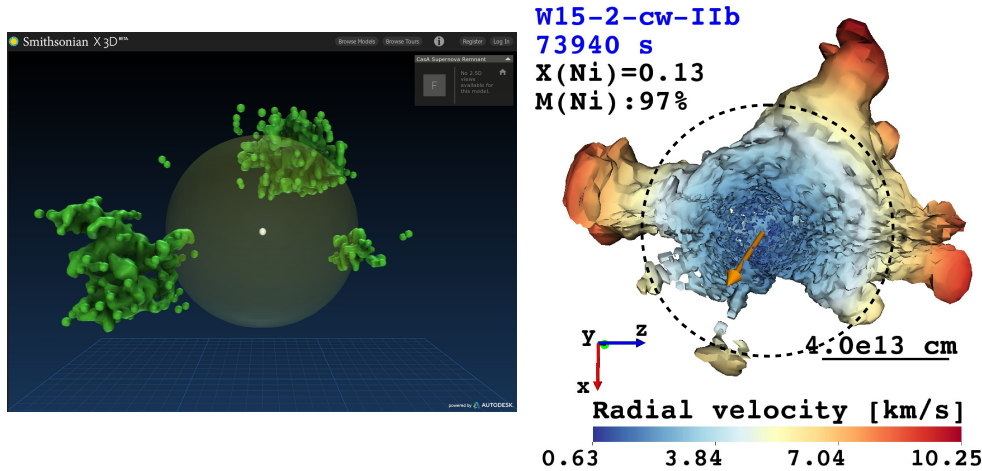


Figure 6. *Left:* Iron K-shell emission around the reverse-shock sphere of Cas A as measured by the Chandra X-ray observatory (DeLaney et al. (2010), Hwang & Laming (2012)). The NS is marked by a white bullet. (Image copied from 3D visualization available at <http://3d.si.edu/explorer?modelid=45>.) *Right:* Distribution of ^{56}Fe in a 3D simulation of a neutrino-driven explosion (Wongwathanarat et al. (2016)). The NS kick direction (red arrow) and the approximate location of the reverse shock (dashed circle, assuming 50% of the iron to be shock heated) are indicated.

served in young SN remnants such as SN 1987A and Cas A. Invoking new features in an ad hoc manner (e.g. “jittering jets”, Soker (2017a)) instead of relying on self-consistently

developing hydrodynamic instabilities that collaborate with the neutrino-heating mechanism, is not necessary.

For SN 1987A neutrino-driven explosions predict the existence of a NS as a compact remnant. In view of a diagnosed explosion energy of $(1.3 - 1.5) \times 10^{51}$ erg, massive fallback is highly unlikely for the progenitors (with He-core masses between 4 and $6 M_{\odot}$) considered for SN 1987A. Because of a maximum NS mass of at least $2 M_{\odot}$ (Antoniadis et al. (2013), Demorest et al. (2010)) the collapse of the compact remnant of a neutrino-driven explosion to a BH can be ruled out. If the existence of a BH in SN 1987A can be proven, radical revisions of our understanding of the SN mechanism would therefore be inescapable (e.g., Blum & Kushnir (2016)).

Acknowledgments. This work was supported by the Deutsche Forschungsgemeinschaft through the Cluster of Excellence EXC 153 “Origin and Structure of the Universe”, by the European Research Council through grant ERC-AdG No. 341157-COCO2CASA. The computations were performed on Hydra of the Max Planck Computing and Data Facility.

References

- Abbott, B.P., et al. 2016, *Phys. Rev. Lett.*, 116, 061102
 Antoniadis, J., et al. 2013, *Science*, 340, 448
 Arnett, D. 1967, *Canadian Journal of Physics*, 45, 1621
 Arnett, W.D., Bahcall J.N., Kirshner R.P., & Woosley, S.E. 1989, *Ann. Rev. Astron. Astrophys.*, 27, 629
 Beck, P.G., et al. 2012, *Nature*, 481, 55
 Bethe, H., & Wilson, J.R. 1985, *Astrophys. J.*, 295, 14
 Blum, K., & Kushnir, D. 2016, *Astrophys. J.*, 828, 31
 Burrows, A. 2013, *Rev. Mod. Phys.*, 85, 245
 Burrows, A., Dessart L., Livne E., Ott, C.D., & Murphy, J. 2007, *Astrophys. J.*, 664, 416
 Colgate, S.A., & White, R.H. 1966, *Astrophys. J.*, 143, 626
 Couch, S.M., & Ott, C.D. 2013, *Astrophys. J. Lett.*, 778, L7
 Couch, S.M., Chatzopoulos, E., Arnett, W.D., & Timmes, F.X. 2015, *Astrophys. J. Lett.*, 808, L21
 DeLaney, T., et al. 2010, *Astrophys. J.*, 725, 2038
 Demorest, P.B., Pennucci, T., Ransom, S.M., Roberts M.S.E., & Hessels, J.W.T. 2010, *Nature*, 467, 1081
 Eggenberger, P., Montalbán J., & Miglio, A. 2012, *Astron. Astrophys.*, 544, L4
 Eggenberger, P., et al. 2016, *Astronomische Nachrichten*, 337, 832
 Endeve, E., et al. 2012, *Astrophys. J.*, 751, 26
 Foglizzo, T., et al. 2015, *Publ. Astron. Soc. Australia*, 32, e009
 Grefenstette, B.W., et al. 2014, *Nature*, 506, 339
 Grefenstette, B.W., et al. 2017, *Astrophys. J.*, 834, 19
 Heger, A., Langer, N., & Woosley, S.E. 2000, *Astrophys. J.*, 528, 368
 Heger, A., Woosley, S.E., & Spruit, H.C. 2005, *Astrophys. J.*, 626, 350
 Hwang, U., & Laming, J.M. 2012, *Astrophys. J.*, 746, 130
 Janka, H.-T. 2012, *Ann. Rev. Nucl. Part. Sci.*, 62, 407
 Janka, H.-T. 2017a, *Astrophys. J.*, 837, 84
 Janka, H.-T. 2017b, *e-print arXiv:1702.08825*
 Janka, H.-T., Melson, T., & Summa, A. 2016, *Ann. Rev. Nucl. Part. Sci.*, 66, 341
 Kawaler, S.D. 2015, *ASP Conference Series*, 493, p. 65; *e-print arXiv:1410.6934*
 Kazeroni, R., Guilet, J., & Foglizzo, T. 2017, *eprint arXiv:1701.07029*
 Kushnir, D., & Katz, B. 2015, *Astrophys. J.*, 811, 97
 Larsson, J., et al. 2016, *Astrophys. J.*, 833, 147

- Lentz, E.J., et al. 2015, *Astrophys. J. Lett.*, 807, L31
- Levan, A., Crowther P., de Grijs, R., Langer, N., Xu, D., Yoon, S.-C. 2016, *Space Science Reviews*, 202, 33
- Melson, T., Janka, H.-T., & Marek, A. 2015, *Astrophys. J. Lett.*, 801, L24
- Melson, T., Janka, H.-T., Bollig, R., Hanke, F., Marek, A., & Müller, B. 2015, *Astrophys. J. Lett.*, 808, L42
- Mösta, P., et al. 2014, *Astrophys. J. Lett.*, 785, L29
- Mösta, P., Ott, C.D., Radice D., Roberts, L.F., Schnetter, E., & Haas, R. 2015, *Nature*, 528, 376
- Moiseenko, S.G., & Bisnovatyi-Kogan, G.S. 2007, *Astrophys. and Space Science*, 311, 191
- Müller, B. 2016, *Publ. Astron. Soc. Australia*, 33, e048
- Müller, B., & Janka, H.-T. 2015, *Monthly Not. R. Astron. Soc.*, 448, 2141
- Obergaulinger, M., & Aloy, M.Á. 2017, *eprint arXiv:1703.09893*
- Roberts, L.F., Ott, C.D., Haas, R., O'Connor, E.P., Diener, P., & Schnetter, E. 2016, *Astrophys. J.*, 831, 89
- Scheck, L., Kifonidis, K., Janka, H.-T., & Müller, E. 2006, *Astron. Astrophys.*, 457, 963
- Soker, N. 2017a, *e-print arXiv:1702.03451*
- Soker, N. 2017b, *e-print arXiv:1703.03673*
- Takiwaki, T., Kotake, K., & Suwa, Y. 2014, *Astrophys. J.*, 786, 83
- Utrobin, V.P., Wongwathanarat, A., Janka, H.-T., & Müller, E. 2015, *Astron. Astrophys.*, 581, A40
- Wilson, J.R. 1985, in: J.M. Centrella, J.M. LeBlanc & R.L. Bowers (eds.), *Numerical Astrophysics* (Boston: Jones and Bartlett Publ.), p. 422
- Wongwathanarat, A., Janka, H.-T., & Müller, E. 2013, *Astron. Astrophys.*, 552, A126
- Wongwathanarat, A., Müller, E., & Janka, H.-T. 2015, *Astron. Astrophys.*, 577, A48
- Wongwathanarat, A., Janka, H.-T., Müller, E., Pllummi, E., & Wanajo, S. 2016, *e-print arXiv:1610.05643*
- Woosley, S.E., & Bloom, J.S. 2006, *Ann. Rev. Astron. Astrophys.*, 44, 507